Electronic Supplementary Material (ESI) for Nanoscale.

Supplementary Information

Unusually large hyperfine structure of the electron spin levels in an endohedral dimetallofullerene and its spin coherent properties

Ruslan B. Zaripov,[1] Yuri E. Kandrashkin,[1] Kev M. Salikhov[1], Bernd Büchner[2,3], Fupin Liu,[2] Marco Rosenkranz,[2] Alexey A. Popov[2] and Vladislav Kataev[2]

[1]Zavoisky Physical-Technical Institute, FRC Kazan Scientific Center of Russian Academy of Sciences, Kazan 420029, Russia

[2]Leibniz IFW Dresden, D-01069, Dresden, Germany

[3]Institute for Solid State and Materials Physics, TU Dresden, D-01062 Dresden, Germany

Synthesis and separation of $Sc_2@C_{80}(CH_2Ph)$

$Sc_2@C_{80}(CH_2Ph)$ was synthesized following the procedure developed by us previously.[1, 2] In brief, arc-discharge synthesis was performed in He atmosphere with graphite electrodes filled with a mixture of Sc_2O_3 and graphite powder. The soot produced in the arc was extracted by boiling in DMF overnight, and the extract solution in DMF was then reacted with excess of benzyl bromide at elevated temperature. At this stage reaction gives a mixture of benzyl-adduct of Sc-EMFs soluble in toluene. This mixture was then separated by a three-step HPLC as presented in Figure S1. The mass spectra presented in Figure S2 confirm the purity of the isolated $Sc_2@C_{80}(CH_2Ph)$ compound. The similarity of the UV-vis-NIR absorption spectra of $Sc_2@C_{80}(CH_2Ph)$ and all other $M_2@C_{80}(CH_2Ph)$ compounds characterized earlier proves that they have the same molecular structure (Figure S3, the spectrum of $Tb_2@C_{80}(CH_2Ph)$ from Ref. 1 is used for comparison)

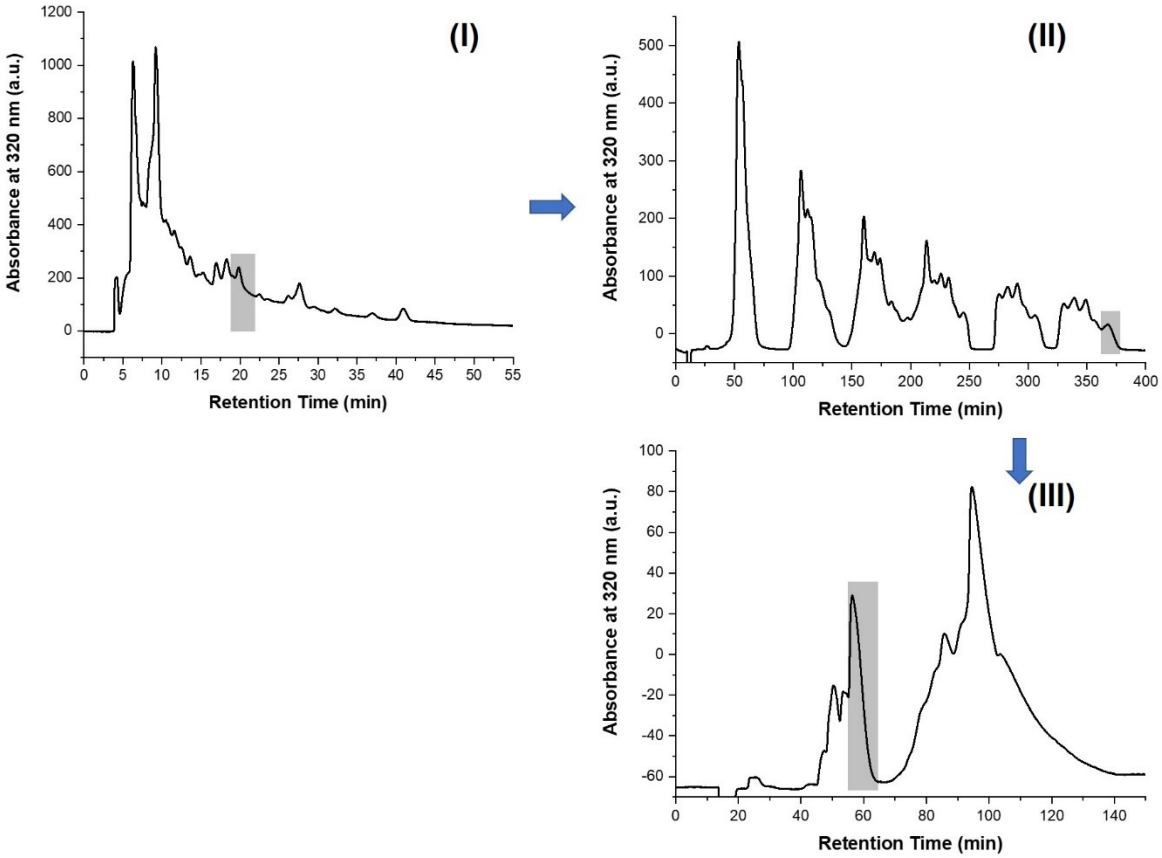

Figure S1. Separation of $Sc_2@C_{80}(CH_2Ph)$. Three steps HPLC separation were required to obtain the pure compound. **(I)** HPLC profile of the mixture of benzyl-derivatized Sc-EMFs. The highlighted fraction contained $Sc_2@C_{80}(CH_2Ph)$ was collected for further separation. HPLC conditions: linear combination of two 4.6 × 250 mm Buckyprep columns; flow rate 1.6 mL/min; injection volume 800 μL; toluene as eluent; 40 °C. **(II)** Recycling HPLC separation of the fraction collected in the first step. The highlighted fraction was collected for further separation (10 × 250 mm Buckyprep column; flow rate 1.5 mL/min; injection volume 4.5 mL; toluene as eluent). **(III)** HPLC separation of the fraction collected in the second step. Pure $Sc_2@C_{80}(CH_2Ph)$ was obtained as the highlighted fraction. (10 × 250 mm Buckyprep-D column; flow rate 1.0 mL/min; injection volume 4.5 mL; toluene as eluent).

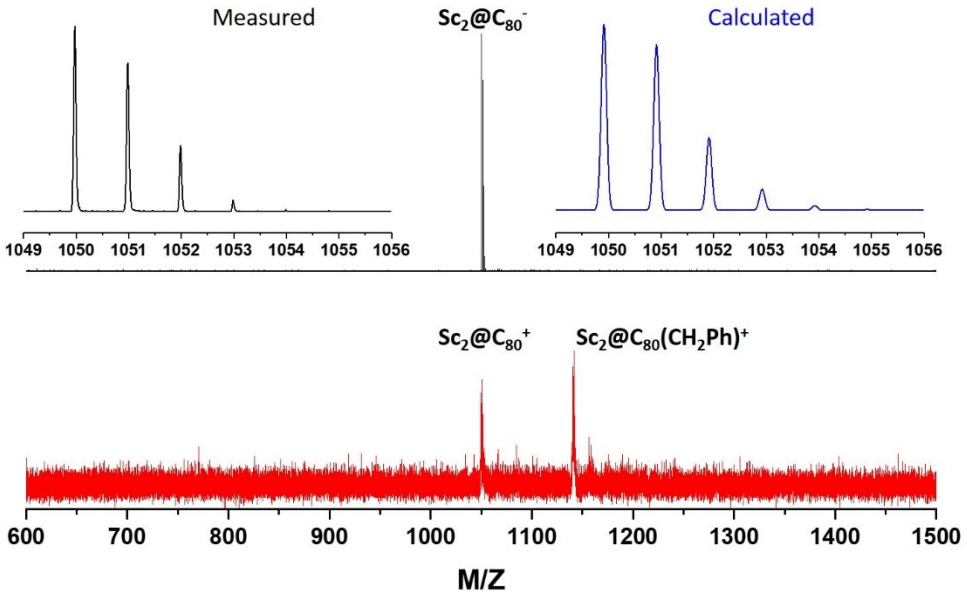

Figure S2. Matrix-assisted laser desorption/ionization time-of-flight (MALDI TOF) mass-spectra of $Sc_2@C_{80}(CH_2Ph)$. Linear negative (top) and positive (bottom) ionization modes. Resolution in positive mode is not high enough for analysis of isotopic distribution. In the negative ion mode, strong fragmentation does not allow for detection of molecular peak, but spectral resolution is sufficient to prove correct isotopic distribution of the $Sc_2@C_{80}^-$ fragment.

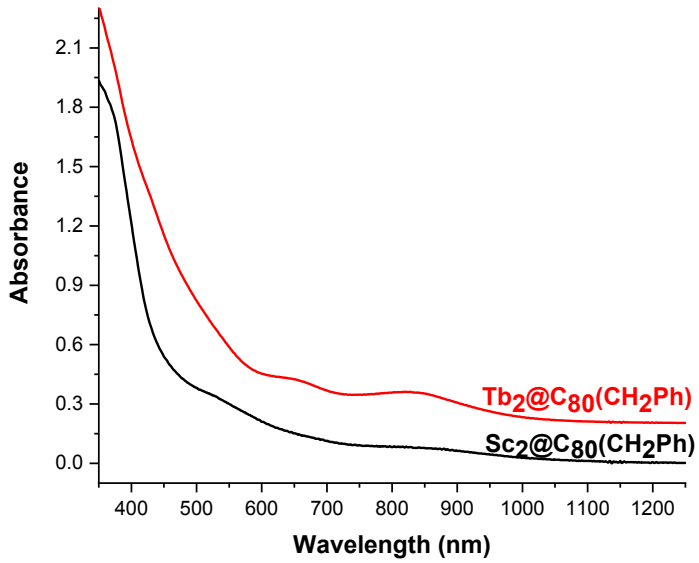

Figure S3. UV-vis-NIR absorption spectra of $Sc_2@C_{80}(CH_2Ph)$ in comparison with $Tb_2@C_{80}(CH_2Ph)$ (room temperature, toluene solution).

Simulation of the X-band EPR spectra of $Sc_2@C_{80}(CH_2Ph)$

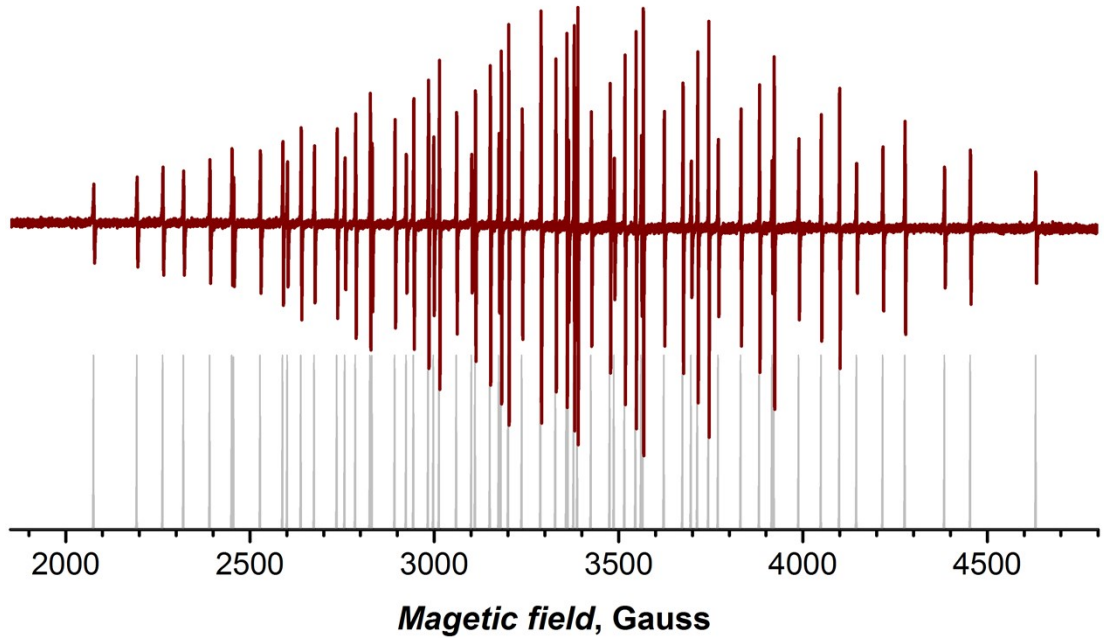

Figure S4. Experimental X-band spectrum of $Sc_2@C_{80}(CH_2Ph)$ measured in toluene at room temperature (top) is compared to the calculated position of the resonance transitions (gray vertical lines). The fit performed with EasySpin software[3] gives $a_{iso}(^{45}Sc)$ =509.5 MHz, g_{iso} = 1.9955

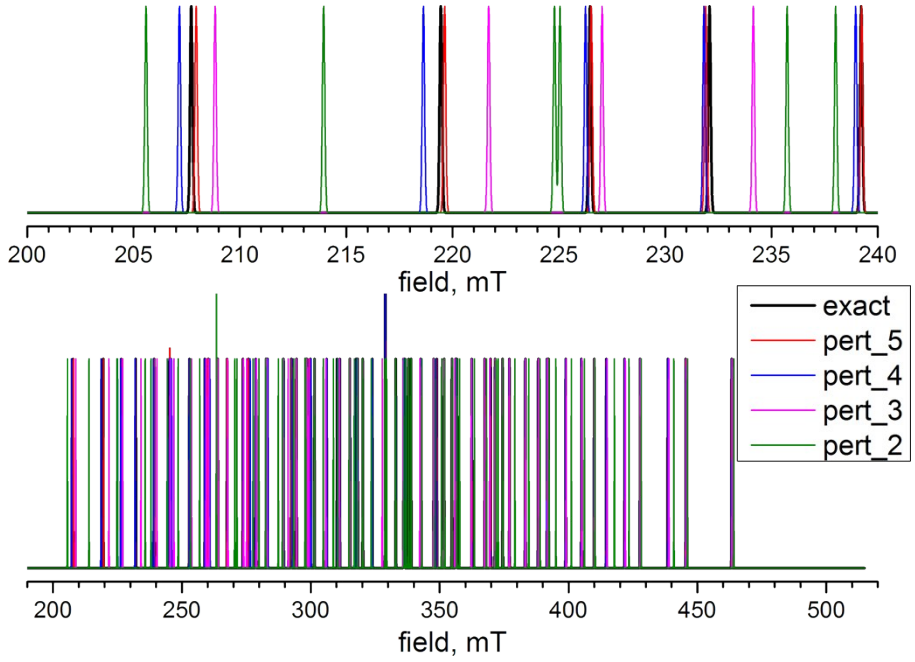

Figure S5. Calculated resonance position of $Sc_2@C_{80}$(CH2Ph) calculated with the "exact" algorithm (black lines) and with perturbation theory of 2nd to 5th order. The upper panel zooms in the low-field range

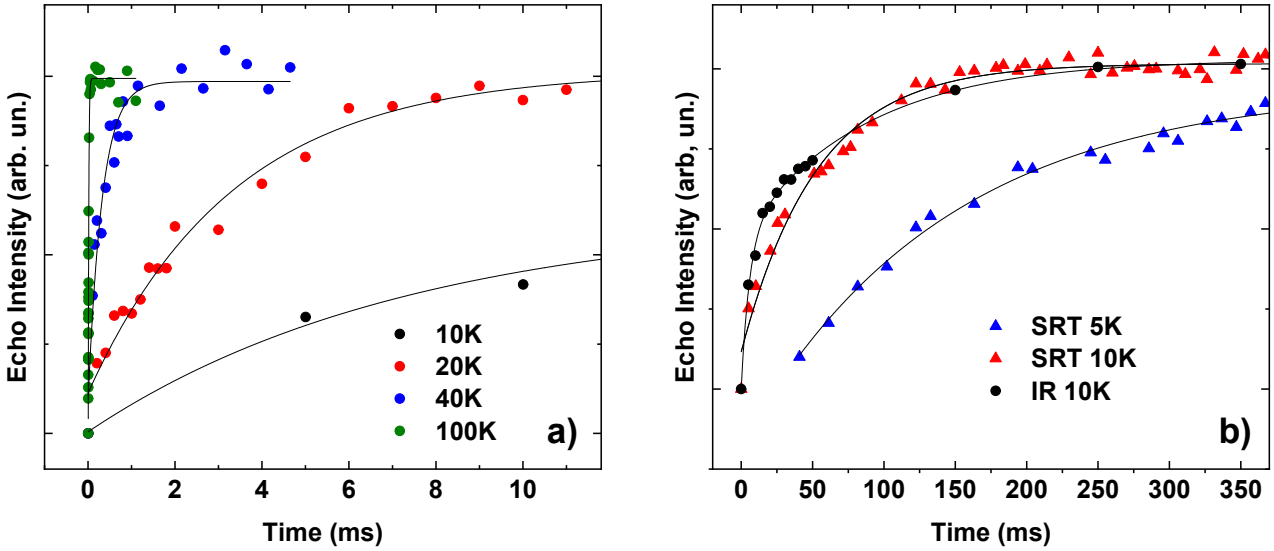

Figure S6. Examples of experimental time dependence of the electron spin echo intensity at different temperatures obtained with **(a)** - the inversion recovery (IR) protocol; **(b)** - the protocol of fast repetition of the pulse sequence with the variable shot repetition time (SRT). Here, the IR curve is added for comparison. As discussed in the main text, the IR protocol is less accurate at low temperatures[4], which causes a discrepancy between the SRT and IR traces at $T = 10$ K. Fits to experimental data in (a) and (b) are shown by solid lines.

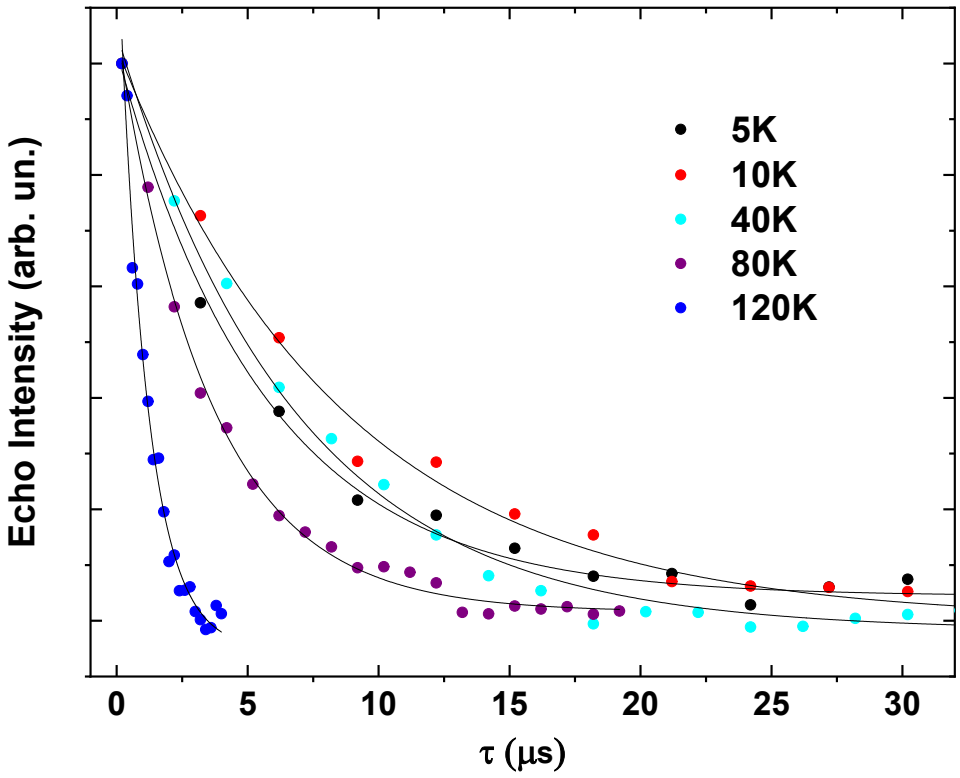

Figure S7. Experimental dependence of the electron spin echo intensity on the inter-pulse delay time τ in the two pulse experiment at different temperatures. Solid lines are fits to experimental data.

Table S1. Phase memory T_m and longitudinal T_1^{IR} and T_1^{SRT} relaxation times at different temperatures. Labels IR and SRT correspond to the inversion recovery method and the protocol of fast repetition of the pulse sequence, respectively.

Temperature, K	**Relaxation times**		
	T_m, **μs**	T_1^{IR}, **μs**	T_1^{SRT}, **μs**
5	12.2±0.8	-	238814.7±23290.0
10	17.0±1.3	32570.0±4664.6	51472.3±4153.3
20	16.7±1.0	3570.3±356.7	5574.5±369.7
40	13.5±0.8	296.4±44.3	-
60	11.6±1.0	76.5±8.5	-
80	7.1±0.3	40.0±6.5	-
100	2.7±0.1	12.8±1.3	-
120	2.2±0.2	26.0±10.7	-

Reference

1. F. Liu, G. Velkos, D. S. Krylov, L. Spree, M. Zalibera, R. Ray, N. A. Samoylova, C.-H. Chen, M. Rosenkranz, S. Schiemenz, F. Ziegs, K. Nenkov, A. Kostanyan, T. Greber, A. U. B. Wolter, M. Richter, B. Büchner, S. M. Avdoshenko and A. A. Popov, *Nat. Commun.*, 2019, **10**, 571.
2. F. Liu, D. S. Krylov, L. Spree, S. M. Avdoshenko, N. A. Samoylova, M. Rosenkranz, A. Kostanyan, T. Greber, A. U. B. Wolter, B. Büchner and A. A. Popov, *Nat. Commun.*, 2017, **8**, 16098.
3. S. Stoll and A. Schweiger, *J. Magn. Reson.*, 2006, **178**, 42-55.
4. A. Schweiger and G. Jeschke, *Principles of Pulse Electron Paramagnetic Resonance*, Oxford University Press, 2001.